ARTICLE

# Analysis of Topographic Change at Mount Sakurajima, South Kyushu, Japan, using JERS-1 SAR Interferometry

Nobuhiro TOMIYAMA[1], Katsuaki KOIKE[2], Masato IGUCHI[3] and Makoto OMURA[4]

[1] Remote Sensing Technology Center of Japan, Minato-ku, Tokyo, Japan. e-mail:tomiyama@restec.or.jp
[2] Graduate School of Science and Technology, Kumamoto University, Kumamoto, Japan.
[3] Sakurajima Volcano Research Center, DPRI, Kyoto University, Kagoshima, Japan.
[4] Department of Environmental Science, Kochi Women's University, Kochi, Japan.

(Received: 10 October 2010; Accepted: 26 November 2010)

**Abstract** : Mount Sakurajima, situated in the southern Kyusyu district of southwest Japan, is known as one of the most active volcanoes in Japan. It has erupted intermittently, ejecting large volumes of volcanic materials including lava, scoria, and ash. We have adopted a SAR interferometry method using JERS-1 images to monitor volcanic activity and estimate accompanying topographic changes in order to mitigate hazard from the inevitable eruptions and debris flows. A map expressing the phase-difference distribution for pairs of images recorded on two acquisition dates is produced for this purpose. This map, obtained by subtracting orbital and topographic fringes from the initial interferogram, is capable of quantifying vertical displacements at each point on the SAR image. Considering the acquisition-date intervals for the images used, three phase-difference maps are generated for the period from January 1996 to March 1997. These show that relatively large displacements occurring along the valleys on the northern slopes of the volcano are common to the three pairs. Because the volcanic activity was low during the period, the displacements may be caused chiefly by the erosion of the surface materials. Differential SAR interferometry is thus thought to be capable of estimating temporal fluctuations of topography during arbitrary periods, detecting regions that are readily aggraded or eroded, and helping to determine the position and dimensions of debris barriers.

**Key words** : Active volcano, L-band, JERS-1, SAR interferometry, Erosion

## 1. Introduction

Monitoring topographic change on a volcano is important for extracting the specific characteristics of its activity and also for investigating local crustal deformation resulting from the regional stress field. Such monitoring can also contribute to reducing vulnerability from volcanic hazards by contributing to eruption forecasts, estimating areas and volumes of pyroclastic deposits, and localizing distributions of volcanic products transported and deposited by rain. Satellite remote sensing has been an effective observation method, and particularly so for active volcanoes with scattered and extensive eruptions. This is because possible surveying equipment sites are limited in terms of both their number and their distribution.

Many remote sensing applications using optical and microwave sensors for volcanic analysis have been reported previously (e.g., Rothery *et al*., 1988; Flynn *et al*., 1994; Mouginis-Mark, 1995; Wooster and Kaneko, 1998; Flynn *et al*., 2001; Saepuloh *et al*., 2010). Although the earth-observation satellites represented by LANDSAT ETM+ and SPOT HRV are useful for detecting volcanic ash clouds, pyroclastic flows, and lava flows based on the multi-spectral nature of the optical sensors on board these satellites, the image quality of these systems is strongly affected by weather conditions. In comparison, synthetic aperture radar (SAR) has proven to be capable of taking fine-scale images regardless of cloud coverage over a target area. Moreover, SAR interferometry ("In-SAR" hereafter) has also been used to construct a digital elevation model (DEM) of volcano and estimate minute topographic changes accompanied by an eruption (Massonnet *et al*., 1995; Moreira *et al*., 1995; Zebker *et al*., 1996; Lu *et al*., 1998; Sigmundsson *et al*., 1999; Remy *et al*., 2003; Tomiyama *et al*., 2004). However, the applications of In-SAR to the time-series analysis of topographic changes for a long period are still limited (Thatcher *et al*., 1997). Such an analysis is essential for volcanic monitoring. In this paper, we present displacements detected for an active volcano between two satellite imaging exercises using Mount Sakurajima of Japan as the target, including an evaluation of the In-SAR technique.

## 2. Eruptive activity of Mount Sakurajima

Mount Sakurajima is an andesitic stratovolcano located at the southern rim of Aira caldera, in southern Kyushu (Fig. 1). A Plinian eruption occurred at the Aira caldera 22 ka and Sakurajima started its activity as a post-caldera cone of the caldera 20 ka (Aramaki, 1984). The eruptive history and geology of Mount Sakurajima are summarized systematically by Kobayashi and Ezaki (1996) and Fukuyama (1978), respectively. The following descriptions mainly follow these references.

Sakurajima is composed of two summit cones, Kita-dake and Minami-dake (Fig. 2). Eruptive activity occurred at Kita-dake until 5 ka, then moved to Minami-dake after that. Since 2 ka, repeated flank and summit eruptions have occurred at the Minami-dake summit crater. Large eruptions occurred on the flank in AD 764, 1471-1476, 1779, 1914 and 1946. Large amounts of lava were extruded and pumice was deposited on the flanks of the volcano in each of these eruptions. In the Bunmei eruption of 1471-1476, 0.7 $km^3$ of pumice was ejected and deposited on the north flank of the volcano. Eruptive activity with Vulcanian explosions at the summit of Minami-dake has continued since 1955. The eruptive activity reached at its peak in 1960 and gradually decreased; however, a strong eruption did occur on October 2, 1972, and more than 400 volcanic explosions occurred in 1974 and 1985. Accompanying the explosions, large amounts of volcanic ash were emitted; in particular, the 1985 eruptions ejected 29 million tons of ash in total. Deposition of the volcanic ash in conjunction with rainfall has frequently caused mud flows, which eroded pumice and other layers formed by previous large eruptions. Eruptive activity has gradually decreased since 1986 and less than 1000 explosions have occurred since 1993.

## 3. Selection of JERS-1 SAR data

Most of Mount Sakurajima is thickly covered by vegetation. For this surface condition, L-band SAR is most effective in producing a complete interferogram, as demonstrated by Koike *et al*. (2002). This is the main reason why we have used JERS-1 L-band SAR data, with microwave wavelengths of 23.5 cm, for topographic change analysis. L-band microwaves can penetrate through foliage and be scattered at the ground surface. The disadvantage for shorter wavelength C-band SAR data, from satellites such as RADARSAT and ERS-1/2, is that it is difficult to produce a complete interferogram due to the large temporal changeability in backscattering intensity of vegetation at those wavelengths.

Mount Sakurajima lies on the right side of the JERS-1 SAR scene of path 49 and row 248. The study area is a square region that is 10 km long in both E-W and N-S dimensions within the scene. We have taken the small eruptions that occurred during March 1996 into account and selected nine instances of the scene acquired before and after the eruptions. The dates of these data range from January 31, 1996, to March 2, 1997.

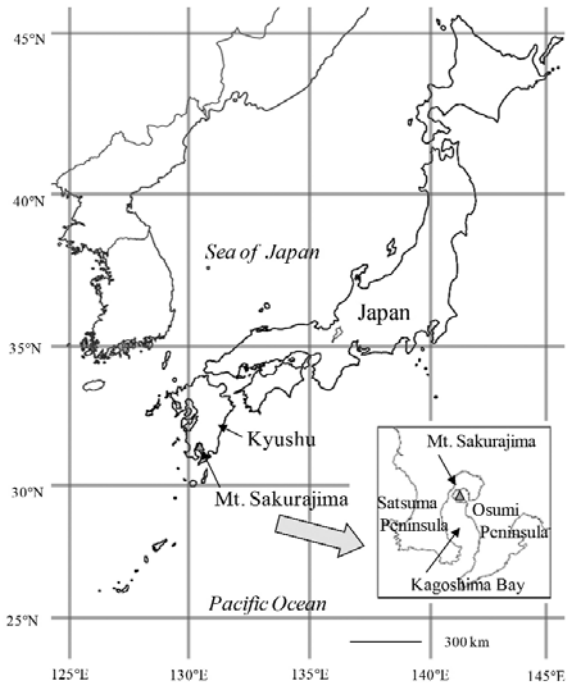


Figure Location of Mount Sakurajima.

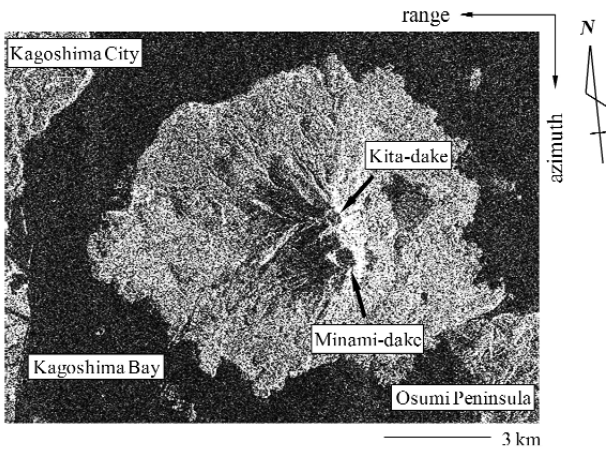


Figure 2. SAR intensity image of single-look complex around Mount Sakurajima produced from the raw signal data in Table 1.

Generally, the coherence of SAR image pairs with long acquisition-date intervals tends to be low. When considering significant topographic changes that are detected from an image pair using the differential In-SAR technique, ambiguities of phase differences hidden in fringe cycles may be large. After considering the baseline length, acquisition-date interval, and coherence of each pair made from the combination of the nine data samplings, three pairs (Table 1) were chosen for the topographic analysis of Mount Sakurajima. These pairs are most suitable for detecting temporal changes on the volcano because the time intervals between earlier and later images for each pair

Table 1. Specifications of three pairs of JERS-1 SAR signal data used in the analysis, average erosion depth, and total precipitation over 10 mm/h.

| Pair no. | Acquisition date | Acquisition date | Baseline length (m) | Average erosion (cm) | Total precipitation (mm) |
|---|---|---|---|---|---|
| <1> | January 31, 1996 | June 11, 1996 | 45 | 7.6 | 167 |
| <2> | July 25, 1996 | October 21, 1996 | 55 | 11.1 | 320 |
| <3> | January 17, 1997 | March 2, 1997 | 307 | 3.6 | 0 |

do not overlap with each other.

Following the procedures by Koike *et al.* (2002), two software applications, EV-SARP and EarthView from Atlantis Scientific Inc., were used for regeneration of the raw signal data and for basic image processing such as a projective affine transformation for co-registration of the two images, removal of orbital fringes, and adaptive filtering to reduce high frequency noise. Figure 2 shows an example of the SAR intensity images around Mount Sakurajima, regenerated by the single-look complex (SLC) type process. A perspective view of Mount Sakurajima is drawn in Figure 6 using a 50-m mesh digital elevation model (DEM), provided by the Geographical Survey Institute of Japan, in order to outline the topographic characteristics.

## 4. Production of phase-difference maps

Differential In-SAR analysis using three SAR datasets consists of three steps: the first is generation of an initial interferogram by coregistering two SLC images; the second is flattening to removes orbital fringes; and the third is removal of topographic fringes from the flattened interferogram and production of a phase-difference map to estimate elevation changes that occurred between the two acquisition dates. Ten tie points selected uniformly on the image pair and the affine transformation of the first-order polynomial were used for the accurate coregistration. Figure 3 shows the flattened interferograms that are superimposed on the intensity images.

According to the orbital information, the baseline lengths (denoted by $B$) of the three pairs are (1) 45 m, (2) 55 m, and (3) 307 m. The differentiation of phase difference ($\phi$) with respect to topographic elevation ($h$), is expressed by:

$$\partial\phi/\partial h = 4\pi \mathrm{B} \cos(\theta - \alpha) / \lambda R \sin\theta \qquad (1)$$

where $\theta$, $\alpha$, $\lambda$, and $R$ are inclination angle of the baseline, off-nadir angle, microwave wavelength, and slant range, respectively. Using this equation, the height differences per fringe cycle for the three pairs in Figure 3 are calculated to be (1) 491 m, (2) 446 m, and (3) 126 m.

The topographic fringes can be estimated by the orbital specifications and the 20-mesh DEM that is interpolated from the original DEM. We use the two-dimensional optimization principle method (Shiono *et al.*, 1987), which constructs the smoothest surface from irregularly spaced data, for the interpolation. As an example, the topographic fringes estimated for pair (3) are shown in Figure 4. It is clear that the fringe patterns correspond to the flattened interferogram obtained from SAR image processing (Fig. 3). These same features were found in the topographic fringes estimated for pairs (1) and (2). Therefore, the flattened interferograms are confirmed to express properly the topography of Mount Sakurajima. The results of removing the estimated topographic fringes from the flattened interferograms are depicted in Figure 5, with the superimpositions on the intensity images.

## 5. Estimation of topographic changes from phase-difference maps

To estimate vertical displacements from the phase-difference map shown in Figure 5, a simple model of topographic change accompanied by pressure change in a magma reservoir beneath the volcano is constructed. This magma reservoir is regarded as a pressure source. Assuming the source reservoir to be spherical, the vertical displacement ($\Delta h$) at a horizontal distance ($R$) from the center of the pressure source can be calculated by the following equation after Yamakawa (1955):

$$\Delta h = \frac{3a^2P}{4\mu}\frac{\mathrm{D}}{(D^2+R^2)^{3/2}} \qquad (2)$$

where $D$, $a$, $\mu$, and $P$ are the depth of the center of the source, the radius of the source, the rigidity of the crust, and the change in pressure, respectively. The values of $D$, a, $\mu$, and $|P|$ are defined as $-10$ km, 1 km, $3\times10^7$ dyn/m$^2$, and $6\times10^{10}$ Pa after those estimated for the volcanic activity of Mount Sakurajima by Mogi (1958).

Two vertical movement patterns accompanied by positive, $P=6\times10^{10}$ Pa, and negative, $P=-6\times10^{10}$ Pa, pressure change, which correspond to uplift and subsidence of the terrain surface, respectively, are considered. Using the DEM of Mount Sakurajima and the general orbit specifications of JERS-1 for the study area, two phase-difference maps were produced, as shown in Figure 6. The center of the pressure source is located just beneath Minami-dake. In both maps, displacement decreases gradually away from the center toward the periphery.

Let the displacements on the southern boundary be the reference; the phase differences of one cycle (0-2π) are colored

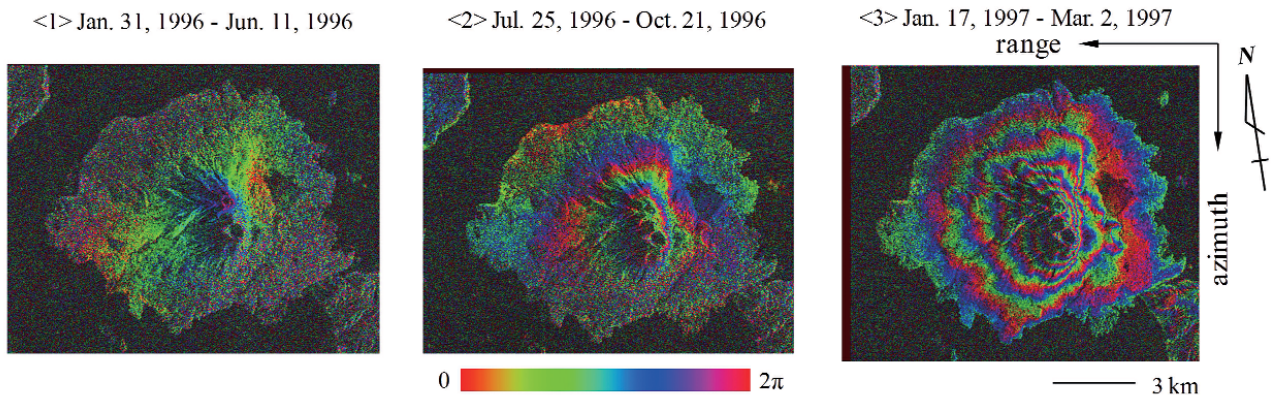


Figure 3. Interferograms obtained by removing orbital fringes from initial interferograms of the three image pairs.

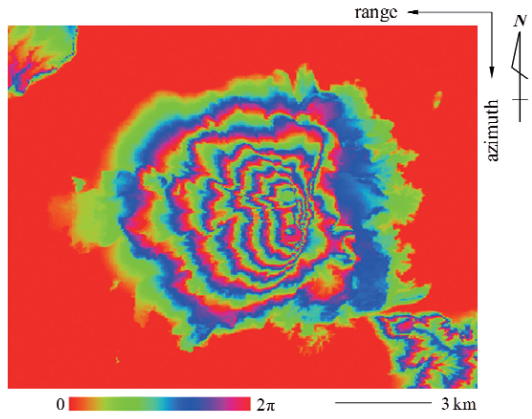


Figure 4. Topographic fringes estimated using the DEM of 20-m mesh and the baseline length of the pair (3).

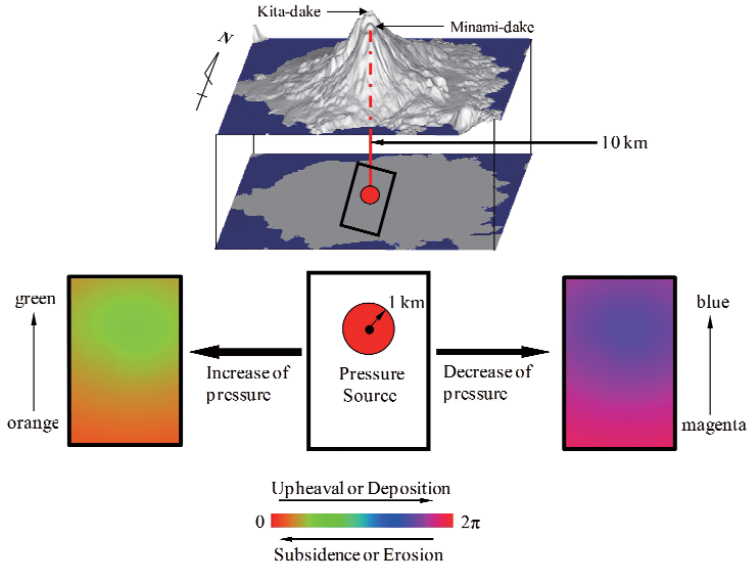


Figure 6. Phase-difference accompanied by upheaval or subsidence of the terrain surface due to the pressure change of a magma reservoir (pressure source). The center of the reservoir is located beneath the active crater (Minami-dake) of Mount Sakurajima as shown in a perspective view of the DEM.

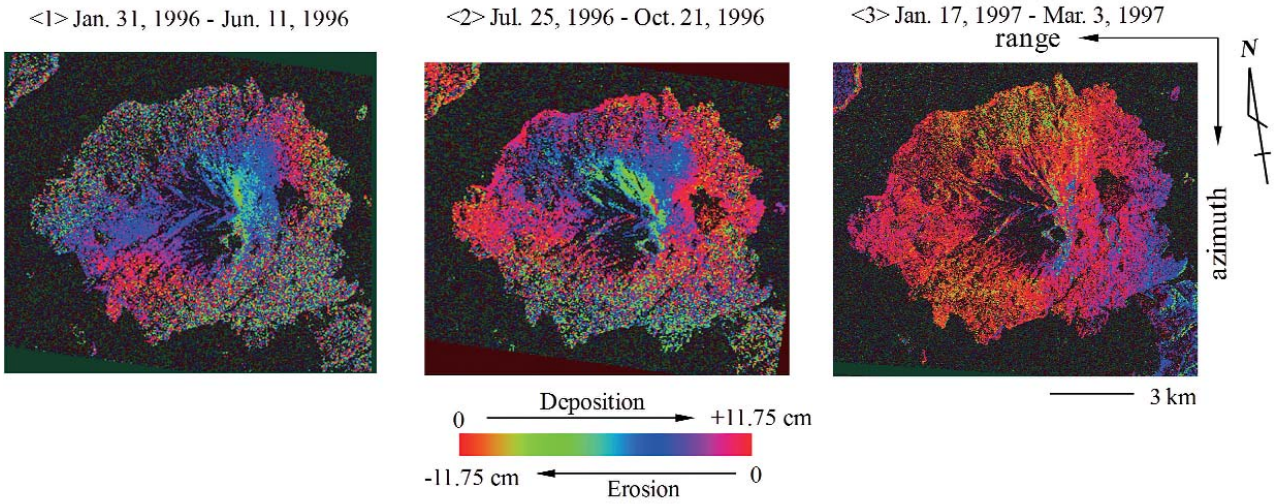


Figure 5. Phase-difference distributions attributed to topographic change in each observation period of the three image pairs.

from red to magenta as indicated by the color bars in Figures 3, 4, 5, 6, and 8. For a movement pattern with a positive P, the displacements near the center are positive as compared to the reference, which expresses the resulting increase in elevations toward the center. These topographic changes can be caused not only by uplift associated with greater volcanic activity, but also by deposition of sediments. The colors of phase differences change from orange on the reference to green in the center. In comparison, a movement pattern with a negative *P* expresses the decrease in elevation that results from subsidence associated with a reduction of volcanic activity and/or erosion of sediments. The colors change from magenta to blue toward the center. Accordingly, the phase-differences from the reference of displacements shown by the color pattern that runs from warm to cold colors correspond to the topographic changes caused by uplift and/or deposition, and those shown by the reverse color pattern correspond to subsidence and/or erosion.

## 6. Results of topographic change analysis and discussion

We set the northeast coast of Sakurajima as the displacement reference because this area can be regarded as having no displacement during the study period. The colors in the three phase-difference maps (Fig. 5) change generally from a reference color of magenta to blue, light blue, and green around the craters. These color orders suggest that topographic changes are related to subsidence and/or erosion based on the above criterion. According to Ishihara (1998), the total volume of volcanic ash falls in 1996 was the smallest since the start of the comprehensive observation in 1974 and the activity of Mount Sakurajima was relatively low. The displacements near the craters were estimated to be larger than several cm, which exceeds the displacements expected due to volcanic activity during a short period. Taking these features into consideration, it is reasonable to conclude that the topographic changes estimated from the phase-difference maps are the result of erosion by rainfall.

Monthly rainfall observations made at a station near Kita-dake are summarized in Figure 7. The total rainfall during the period of each pair increases from pair (3) to pair (1) to pair (2). While the portions colored by green around the craters that show relatively large displacements are not seen in the phase-difference map for pair (3), those are the most conspicuous for the map for pair (2). These relationships between the rainfall and the estimated displacements confirm that erosion is the main cause of topographic change.

Figure 8 is an enlargement of the phase-difference map around the craters obtained from image pair (3). Topographic changes caused by the deposition of volcanic products are inferred only on the western slopes of the continuingly active Minami-dake (the region enclosed by an ellipse in Figure 8).

Although some of the phase-differences may be an artifact of the weather conditions, e.g., as a result of the delay of microwaves due to increased water vapor of the air, note that the erosion amounts estimated for the northern Kita-dake are relatively large and common to the three pairs and the portions with the greatest amounts are distributed linearly. The northern parts of Kita-dake are overlain primarily by pumice. Therefore, these areas are easily eroded as compared to the areas in the south that are overlain chiefly by lave and deep erosional valleys are developed as shown in Figure 9. Volcanic products tend to be deposited preferentially on the southwestern slopes as a result of the weather conditions, which is one of the factors affecting the distribution of erosion.

Figure 10(A) depicts the sum of the displacements estimated during the three periods. These displacements generally correspond to lower elevations on March 2, 1997, as compared to those on January 31, 1996. We find that the aligned features trending NW-SE on the northern slopes of Kita-dake have erosion amounts greater than 20 cm. These features are superimposed on the DEM as shown in Figure 10(B). The agreement in the positions of the large displacements and deep valleys seems to be good. Consequently, the erosion of surface material was greater that the total deposition even considering the small eruptions that occurred in March 1996. The valleys are capable of accumulating thick deposits of volcanic material, which in turn enables high levels of erosion to occur there as well.

To expand the discussion on the effect of rainfall on erosion, erosion depths were averaged for the gullies in the region for each SAR data pair (Figure 8). These depths were correlated with the total precipitation corresponding to the timing of each data pair. Here, we selected rainfall periods with precipitation rates higher than 10 mm/h, because most debris flows on Mount Sakurajima are known to be triggered by rainfall of this intensity. Although the number of data is limited to only three, Figure 11 shows a strong linear correlation between the average erosion depth in gullies and the total precipitation. This trend suggests that the erosion events are mainly caused by debris flows.

In addition, Jitousono *et al*. (1999) reported that average erosion speed in a river basin on the northern slope of Kita-dake was estimated to be about 1.7 cm/y in 1997 based on field observations of material in the river water and flow rate of the rivers. This rate assumes that the ground surface of the basin was eroded at a constant rate. Because this is a spatial average, the magnitude is smaller than the erosion depth for pair (3) in the gullies. Therefore, the order of erosion speed detected by Differential In-SAR may be harmonious with the field observations.

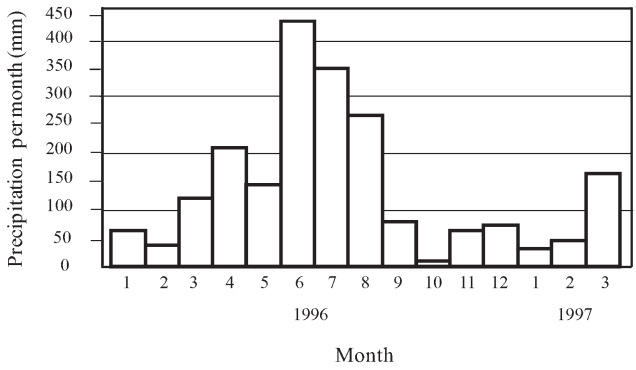


Figure 7. Monthly rainfall observed at a station near Kita-dake.

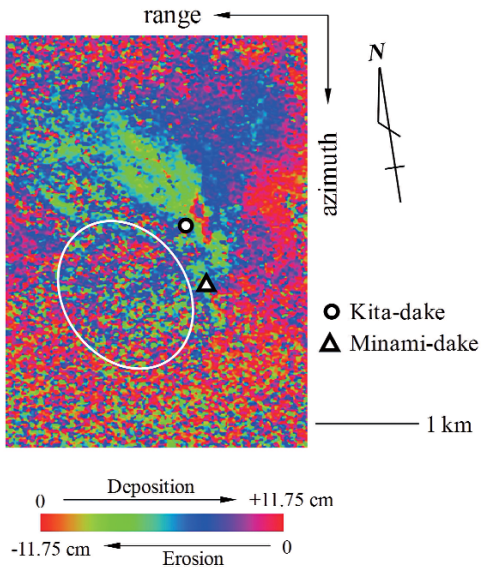


Figure 8. Enlargement of the phase-difference map around the craters obtained though the image pair (3). The region enclosed with an ellipse implies the topographic changes with the deposition of volcanic products.

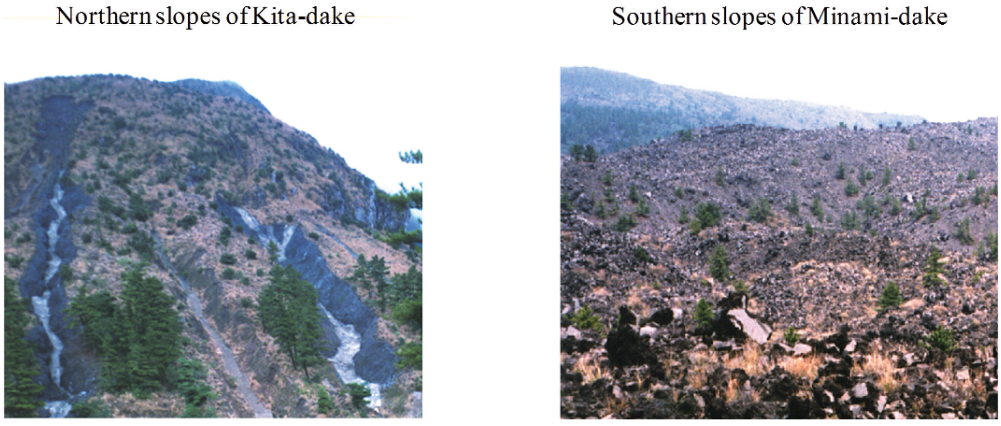


Figure 9. Landscapes of the northern slopes of Kita-dake and the southern slopes of Minami-dake.

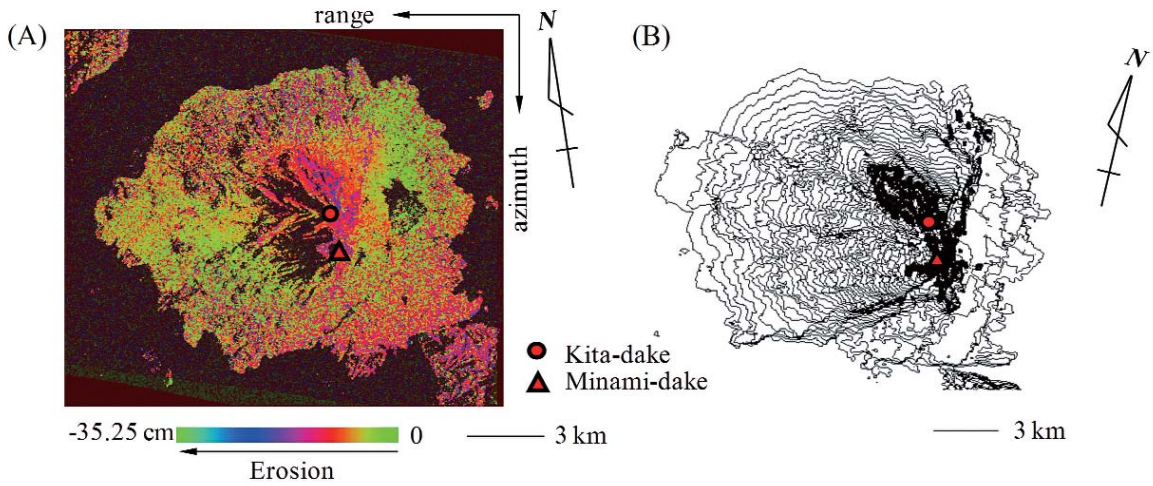


Figure 10. (A) Sum of the displacements estimated during the three periods, which means generally the subtraction of the elevations on March 2, 1997, from those on January 31, 1996, and (B) superimposition of the portions with displacements larger than 20 cm

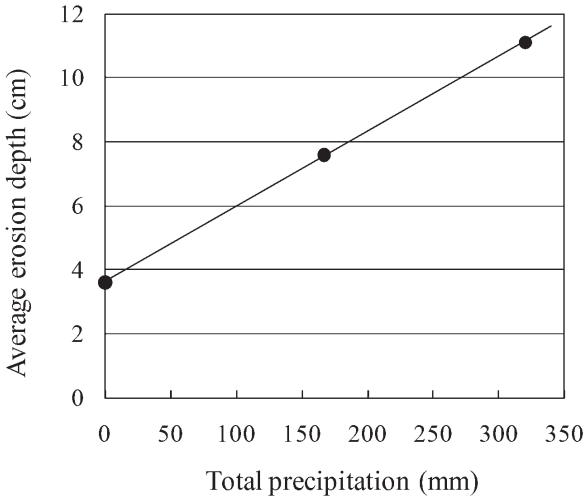


Figure 11. Relationship between the average of erosion depth in gullies and total precipitation over 10 mm/h for each corresponding data-pair period. The regression line for this relationship is overlapped.

## 7. Conclusions

A differential In-SAR technique using JERS-1 SAR images and a 20-m DEM mesh has been successfully applied to analyze topographic change on Mount Sakurajima in southern Japan. From January 1996 to March 1997, during a period of gentle volcanic activity, overall topographic changes were chiefly attributed to the erosion of surface materials by rainfall. The northern slopes of the volcano, overlain widely by pumice, were estimated to have relatively large changes. In particular, changes in elevation exceeding 20 cm were located along the valleys in this area using the superimposition of the displacement map and the DEM. In addition to monitoring volcanic activity, differential In-SAR can contribute to the reduction of vulnerability from volcanic hazards by estimating temporal fluctuations of topography during arbitrary periods, detecting regions where erosion or deposition is preferential, and helping to determine the positions and dimensions of debris barriers.

**Acknowledgments:** The Ministry of International Trade and Industry of Japan and the JAXA (formerly NASDA) retain the ownership of JERS-1 data. The authors wish to express their sincere gratitude to Mr. Shingo Maniwa, formerly a student at the Graduate School of Science and Technology, Kumamoto University, for his help with the SAR image processing.

## References

Aramaki, S. (1984) Formation of the Aira caldera, southern Kyushu, ~22,000 years ago. *J. Geophys. Res.*, vol. 89, no.B10, pp. 8485-8501.

Flynn, L. P., Mouginis-Mark, P. J. and Horton, K. A. (1994) Distribution of thermal areas on an active lava flow field: Landsat observations of Kilauea, Hawaii, July 1991. *Bull. Volcanol.*, vol. 56, no.4, pp. 284-296.

Flynn, L. P., Harris, A. J. L., Wright, R. (2001) Improved identification of volcanic features using Landsat 7 ETM+. *Remote Sensing of Environment*, vol. 78, no.1, pp. 180-193.

Fukuyama, H. (1978) Geology of Sakurajima volcano, southern Kyushu. *Journal of the Geological Society of Japan*, vol. 84, no.6, pp. 309-316 (in Japanese with English abstract).

Ishihara, K. (1998) Summary. Report of 9th Joint Observation of Geophysics and Geochemistry on Sakurajima Volcano: pp. 127-132.

Jitousono, T., Shimokawa, E. and Teramoto, Y. (1999) Runoff Characteristics of Debris Flows and Floods in Sakurajima Volcano. *Water Sciences*, vol. 42, no.6, pp.70-83 (in Japanese).

Kobayashi, T. and Ezaki, M. (1996) Eruptive history of Sakurajima Volcano, southern Kyushu, Japan. *Summaries of Resarches Using AMS at Nagoya University (CCR)*, vol. 7, pp. 70-81 (in Japanese with English abstract).

Koike, K., Omura, M., Iguchi, M., Matsunaga, N. and Tomiyama, N. (2002) Detection of distribution of the 1998 pyroclastic flows at Merapi Volcano, Central Java, Indonesia using RADARSAT images. *Asian Journal of Geoinformatics*, vol. 2, no.4, pp. 9-18.

Lu, Z., Mann, D. and Freymueller J. (1998) Satellite radar interferometry measures deformation at Okmok volcano. *EOS*, vol. 79, no.39, pp. 466-468.

Massonnet, D., Briole, P. and Arnaud, A. (1995) Deflation of Mount Etna monitored by spaceborne radar interferometry. *Nature*, vol. 375, no.6532, pp. 567-570.

Mogi, K. (1958) Relations between the eruptions of various volcanoes and the deformations of the ground surface around them. *Bull. Earthq. Res. Inst.*, vol. 36, no.2, pp. 99-134.

Moreira, J., Schwäbisch, M., Fornaro, G., Lanari, R., Bamler, R., Just, D., Steinbrecher, U., Brei, H., Einder, M., Franceschetti, G., Geudtner, D. and Rinkel, H. (1995) X-SAR interferometry: first results. *IEEE Trans. Geosci. Remote Sensing*, vol. 33, no.4, pp. 950-956.

Mouginis-Mark, P. J. (1995) Preliminary observations of volcanoes with the SIR-C radar. *IEEE Trans. Geosci. Remote Sensing*, vol. 33, no.4, pp. 934-941.

Remy, D., Bonvalot, S., Briole, P. and Murakami, M. (2003) Accurate measurements of tropospheric effects in volcanic areas from SAR interferometry data: application to Sakurajima volcano (Japan). *Earth and Planetary Science Letters*, vol. 213, no.3-4, pp. 299-310.

Rothery, D. A., Francis, P. W. and Wood, C. A. (1988) Volcano monitoring using short wavelength infrared data from satellites. *J. Geophys. Res.*, vol. 93, no.B7, pp. 7993-8008.

Saepuloh, A., Koike, K. Omura, M., Iguchi, M. and Setiawan,

A. (2010) SAR- and gravity change-based characterization of the distribution pattern of pyroclastic flow deposits at Mt. Merapi during the past 10 years, no.2. *Bull. Volcanol.*, vol. 72, pp. 221-232.

Shiono, K., Wadatsumi, K. and Masumoto, S. (1987) Numerical determination of the optimal bedding plane. *Geological Data Processing*, no. 12, pp. 299-328 (in Japanese with English abstract).

Sigmundsson, F., Durand, P. and Massonnet, D. (1999) Opening of an eruptive fissure and seaward displacement at Piton de la Fournaise volcano measured by RADARSAT satellite radar interferometry. *Geophys. Res. Lett.*, vol. 26, no.5, pp. 533-536.

Thatcher, W. and Massonnet, D. (1997) Crustal deformation at Long Valley caldera, eastern California, 1992-1996 inferred from satellite radar interferometry. *Geophys. Res. Lett.*, vol. 24, no.20, pp. 2519-2522.

Tomiyama, N., Koike, K. and Omura, M. (2004) Detection of topographic changes accompanied with volcanic activities of Mt. Hossho by D-InSAR. *Advances in Space Science*, vol. 33, no.3, pp. 279-283.

Wooster, M. J. and Kaneko, T. (1998) Satellite thermal analyses of lava dome effusion rates at Unzen Volcano, Japan. *J. Geophys. Res.*, vol. 103, pp. 20935-20947.

Yamakawa, N. (1955) On the strain produced in a semi-infinite elastic solid by an interior source of stress. *J. Seismological Society of Japan (Zisin)*, vol. 8, no.2, pp. 84-98 (in Japanese with English abstract).

Zebker, H., Rosen, P., Hensley, S. and Mouginis-Mark, P. J. (1996) Analysis of active lava flows on Kilauea volcano, Hawaii, using SIR-C radar correlation measurements. *Geology*, vol. 24, no.6, pp. 495-498.

要　旨

**JERS-1 干渉 SAR を用いた桜島火山の地形変化解析**

：冨山 信弘[1]・小池 克明[2]・大村 誠[3]・井口 正人[4]

火山体の地形変化の把握は，火山活動や広域応力場に起因した地殻変動の特徴の抽出において重要であり，火山噴出物量の見積もり，および火山噴火後の降雨による流出量の推定という火山防災の分野にも貢献できる。LANDSAT や SPOT に代表される光学センサによる観測は，火山噴出物の分布範囲の特定に利用できるが，地形や地形変化の詳細，かつ定量的な評価が困難である。そこで，全天候型である合成開口レーダ（SAR）データに注目し，活動が継続的な桜島火山を対象に選んで，JERS-1 衛星データの干渉処理により火山体の地形変化の抽出を行った。1996 年 1 月～1997 年 3 月の比較的連続する 3 つのデータペアで良質の干渉画像が得られたので，解析はこの期間に限定した。1996 年の火山活動は穏やかであり，しかも変位量の大きな部分は侵食谷の位置に対応しているので，干渉 SAR によって推定される地形変化は主に侵食に起因すると考えられた。3 ペアでの変位量を加算した結果から，対象期間では侵食が優勢であり，北岳の北側で 20 cm 以上の侵食量が推定でき，侵食量の大きい部分が南北方向に伸びていることが見出された。また，南西側の斜面では火山噴出物の供給が大きいので，侵食量は相対的に小さいことなども明らかになった。

キーワード：活火山，L バンド，JERS-1，干渉 SAR，侵食

[1] リモート・センシング技術センター
[2] 熊本大学大学院自然科学研究科
[3] 京都大学防災研究所火山活動研究センター
[4] 高知女子大学環境科学部